Simulation study about the geometry of electrode-electrolyte contact in a SOFC

F. Delloro · M. Viviani

Abstract We tested, by means of simulations, the idea of a patterned contact between composite electrode and electrolyte of a SOFC. Simulation results show that the patterned studied geometry can improve the performance of the assembly in "intermediate" conditions, *i.e.* when there are neither ohmic nor kinetic limitations. The gain reached up to 45 % in terms of current density drawn, with respect to a standard flat contact.

Keywords Solid oxide fuel cell · Composite electrode · Electrode-electrolyte contact · Modeling · Simulation · Optimization

1 Introduction

Current research in Solid Oxide Fuel Cells (SOFC) systems is mainly focused on the optimization of materials and fabrication techniques. In fact lowering cost and improving durability and performance are required to reach commercial standards and bring SOFC systems to industrial production scale. Particular attention is given to electrodes, which have to exploit several mansions, *i.e.* reaction and transport of electrons, ions and gaseous species. Therefore materials used for electrodes have to fulfill a number of requirements: catalyze the reaction, optimize the volumetric density of active sites, assure a sufficient gas phase transport through the pores, minimize ohmic losses due to ionic and electronic transport. The difficulties in the optimization of such a material are clearly understandable looking at number and diversity of these requirements.

F. Delloro (✉)
Centre des Materiaux, Ecole des Mines de Paris,
Evry, France
e-mail: francesco.delloro@ensmp.fr

M. Viviani
Institute for Energetics and Interphases, CNR,
via De Marini 4,
16149 Genova, Italy

In SOFC electrodes, electrochemical semi-reactions involve at the same time ions, coming from the ionic conducting phase, electrons, coming from the electronic conducting phase, and gas species, coming from the pores. Thus, reactions can take place only at the contacting perimeter between those three materials, namely the triple phase boundary (TPB). Mixed ionic and electronic conductors (LSC [1], LSCF [2], BSCF [3] for the cathode, Fe-doped Ceria [4], LSCM [5] for the anode), as well as mixtures of electronic and ionic conducting materials have been widely studied and used to improve TPB [6]. In fact the main advantage of using a composite electrode, made up of porous materials conducting both ions and electrons, is to increase greatly active triple phase boundary (TPB) length. Consider an electrode made with electronic conductor only. TPB is located at the interface with the electrolyte. For a composite electrode, instead, TPB is spread all over the volume, given that percolating paths exist within each phase. The importance of TPB length is readily explained looking at the typical kinetics of an electrodic process, *i.e.* the Butler-Volmer expression (see for example [7] or Eq. 14 below). The exchange current density can be written as a function of the active TPB length:

$$i_V^0 = i^0 \ell_{aTPB} \tag{1}$$

where ℓ_{aTPB} [m/m^3] is the active TPB length density and i^0 [A/m] is the exchange current density per unit TPB length, depending on temperature, gas composition and material. A problem arising in the development of mixed and porous materials is the low ionic conductivity, compared to the pure dense conductor. Especially when reaction is spread in a considerable part of the volume, ohmic drop due to ionic transport in the electrode can heavily affect the performance of the cell.

In this paper we present a strategy for enhancing the performance of the cell. Our idea consists in designing a structured contact between electrode and electrolyte, instead of the usual flat one. The particular type of roughness

introduced at the interface is shown to be theoretically advantageous to cell performances. We investigated our idea by means of 2D finite-element simulations.

In Fig. 1 some examples of simulation domains are given, where the *stem* is clearly visible (this is how we decided to call the electrolyte rectangle in the electrode area). Its height is in the range 10–40 μm. We applied periodic boundary conditions, so that each simulation domain has to be considered as a repeating unit. Then each stem in Fig. 1 represents the microscopic element of the surface regular roughness. Given these periodic boundary conditions, the electrode-electrolyte contact area is infinite and the results are given in terms of current densities, *i.e.* for unit surface area. In the simulations we compared the performance of a conventional flat electrode-electrolyte contact with the structured one, in a wide range of conditions.

Having to fix some of the simulation parameters (e.g. conductivities, exchange current density), we chose to test our idea on the cathode side of a hydrogen fed SOFC, which is a main source of overpotential in the cell. The cathode is a porous layer composed of a Lanthanum Strontium Manganite (LSM) and Yttria-stabilized Zirconia (YSZ) mixture, the most conventional and stable couple of materials for application in SOFCs [8–10].

Results obtained are of general interest for all kinds of reacting layers. For example, the same technique can be applied to the "central membrane" of the IDEAL-cell (see [11] and companion papers).
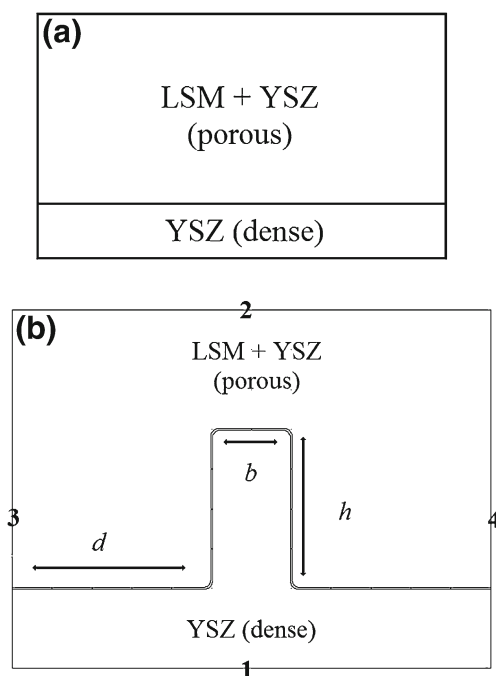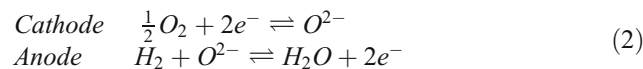

Fig. 1 (*left*) Reference simulation domain: the flat contact. (*right*) stem geometry and parameters to be varied. Horizontal size of the stem (*b*) was fixed to 20 μm in the simulations, while *d* and *h* were varied in the range 10–40 μm

2 Mathematical model

2.1 Introduction

The overall fuel cell reaction $\left(H_2 + \frac{1}{2} O_2 \rightleftharpoons H_2O\right)$ is separated into 3 parts, one (oxygen reduction) taking place at the cathode and the others at the anode.

$$
\begin{aligned}
Cathode \quad & \tfrac{1}{2} O_2 + 2e^- \rightleftharpoons O^{2-} \\
Anode \quad & H_2 + O^{2-} \rightleftharpoons H_2O + 2e^-
\end{aligned}
\tag{2}
$$

We will focus on the cathodic electrochemical reaction only (2), having left the anode out of our simulation domain.

The electrolyte is a dense ion-conducting layer (YSZ). The cathode is a composite porous layer, made of a mixture of ion-conducting particles (YSZ) and electron-conducting particles (LSM). Here, electrochemical reduction of oxygen can only take place in the proximity of a triple phase contact, where molecular oxygen, coming from porosity, and electrons, coming from electronic conducting phase, can meet to form oxygen ions close to the ionic conductor material, which constantly carries oxygen away from the reaction sites towards the electrolyte.

2.2 Model assumptions

The model is based on the following assumptions:

1) Steady state conditions.
2) Temperature is uniform throughout the assembly, *i.e.* heat effects are neglected.
3) The porous electrodes are treated as continuum of the three involved phases. The transport within each phase (gas species, electrons and oxygen ions, respectively) is described using effective transport coefficients.
4) Electronic resistivity of LSM is neglected, being 2 orders of magnitude lower than the ionic resistivity of YSZ (see for example [12]).
5) No mixed electronic-ionic conduction in either the electron-conducting phase or the ion-conducting phase.
6) No electronic current across the cathode-electrolyte interface.
7) Electrochemical reaction kinetically limited by a single step, e.g. the transfer of a single electron, with no other limitation (e.g. adsorption, dissociation, migration), thus resulting in a standard B-V kinetic.

Notice that there are 3 variables involved in our PDE system: ϕ_{YSZ} (potential in ionic conductive phase), c_O and c_N (oxygen and nitrogen partial pressures in the gas phase).

2.3 Transport equations

Recalling assumption 4), we neglected the ohmic drop in the electron-conducting phase, so we can consider the potential

of this phase fixed to a reference value. This simplifies our calculations, since also the potential difference between LSM and YSZ, $\phi = \phi_{YSZ} - \phi_{LSM}$, depends only by ϕ_{YSZ}.

Continuity equation for oxygen ions can be written:

$$\nabla \cdot \overrightarrow{N}_O = i_V/F \qquad (3)$$

where i_M^V is the volumetric current density corresponding to the volumetric reaction rate of oxygen reduction, through Eq. 2. Under stationary conditions, the molar flux of oxygen ions is associated to current density in the conducting phase, which is related to the potential difference through the Ohm law.

$$\overrightarrow{N}_O = \frac{\overrightarrow{i}}{2F} = \frac{\sigma_{YSZ}^{eff}}{2F} \nabla \phi_{YSZ} \qquad (4)$$

Since the electrode is porous, we have to consider effective conductivity, which is related to the dense material property as:

$$\sigma_{YSZ}^{eff} = \frac{\sigma_{YSZ}}{q} \quad \rho_{YSZ}^{eff} = q\rho_{YSZ} \qquad (5)$$

We introduced the effectiveness factor q, whose effect is studied in a set of dedicated simulations and results will be shown later.

Regarding the gas phase transport, we assume the cathode compartment fed by air and consider cathodic atmosphere composed only by oxygen and nitrogen. We decided to apply the Dusty Gas Model (DGM in the following) equations for 2 species to describe mass transport in the gas phase. The model is presented in [13], but the revision of the paper by the authors revealed an error, corrected in Eq. 12 in the present paper.

For each species the total molar flux is given by the sum of diffusion and of permeation fluxes. Total flux $N_i = N_i^f + N_i^d$ appears in the continuity equation for species i:

$$S_i = \nabla \cdot \overrightarrow{N}_i \qquad (6)$$

where ε is the porosity and S_i are source/sink terms. Steady state diffusion is described by the following set of equations:

$$\frac{\overrightarrow{N}_i^d}{D_i^k} + \sum_{\substack{j=1 \\ j \neq i}}^{n} \frac{y_j \overrightarrow{N}_i^d - y_i \overrightarrow{N}_j^d}{D_{ij}^m} = -\nabla(c_T y_i) \qquad (7)$$

where the effective Knudsen diffusion coefficient of component i, D_i^k, and the effective bulk diffusion coefficients of pairs i-j, D_{ij}^m, are defined as:

$$D_i^k = \psi \langle r \rangle \frac{2}{3} \left(\frac{8R_g T}{\pi M_i}\right)^{1/2} \quad D_{ij}^m = \psi D_{ij}^m \qquad (8)$$

ψ is the ratio porosity over tortuosity, $\langle r \rangle$ the mean pore radius and M_i the molar mass of species i, D_{ij}^m is the binary diffusion coefficient, given in [14] as

$$D_{ij}^m = \frac{0.00143 \, T^{1.75}}{p M_{ij} \left(V_i^{1/3} + V_j^{1/3}\right)^2} \quad M_{ij} = 2\left(M_i^{-1} + M_j^{-1}\right)^{-1}$$

V_i being the special *Fuller et al.* diffusion volume.

For the permeation flux we use the Darcy equation:

$$\overrightarrow{N}_i^f = -\frac{B y_i p}{\mu} \nabla c_T \qquad (9)$$

where the permeability B can be calculated as a function of the morphological properties of the membrane by using empirical expressions, as the Blake-Kozeny one:

$$B = \frac{d_p^2}{72\tau} \frac{\varepsilon^3}{(1-\varepsilon)^2} \qquad (10)$$

μ is the gas mixture viscosity, given in [14] as

$$\mu = \frac{\mu_O c_O M_O^{1/2} + \mu_N c_N M_N^{1/2}}{c_O M_O^{1/2} + c_N M_N^{1/2}}$$

Using Eqs. 7 and 11 in Eq. 6, we come to a linear expression:

$$-\nabla c_i = \sum_j F_{ij} \overrightarrow{N}_j \qquad (11)$$

Matrix elements are given in [13], but there is a mistake: the wrong version has α_i in place of α_j in the first Eq. 12. The correct formulation is:

$$\begin{aligned}
F_{ij} &= -\frac{c_i}{c_T D_{ij}^m} + \frac{c_i \alpha_j}{D_i^k} \quad i \neq j \\
F_{ii} &= \frac{1}{D_i^k} + \frac{1}{c_T} \sum_{j \neq i} \frac{c_j}{D_{ij}^m} + \frac{c_i \alpha_i}{D_i^k} \\
\alpha_i &= -\frac{B/D_i^k}{1 + B \sum_j c_j/D_j^k}
\end{aligned} \qquad (12)$$

Inversion of Eq. 11 enables us to write continuity Eq. 6 for the gas components as a function of concentrations only:

$$S_i = \nabla \cdot \left(\sum_j F_{ij}^{-1} \nabla c_j\right) \qquad (13)$$

Equation 13, together with Eq. 6 for the potential in the ion conducting phase, constitute a set of PDEs which can be solved in the simulation domains, given appropriate boundary conditions. The equations are coupled by reaction source/sink terms S_i, which in our case can be written, due to mass and charge conservation: $S_O = i_V/2F$, $S_N = 0$.

2.4 Macro-kinetic model

Assuming that in the oxygen reduction there is a single rate determining step and that it is an electron transfer process, then it can be shown that the reaction kinetic is of the Butler-

Volmer type:

$$i_V = i_V^0 \left[\exp\left(\alpha_M \frac{F}{RT} \eta_{act} \right) - \exp\left(-(1 - \alpha_M) \frac{F}{RT} \eta_{act} \right) \right]$$

(14)

where i_V is the local volume-specific reaction rate, i_V^0 the volume-specific exchange current density, which depends on the microstructure as shown in Eq. 1. η_{act} is the activation overpotential defined such that a positive value leads to water production. The symmetry factor α_M is fixed to 0.5. In the simulations we explored a wide range of variation of the kinetic parameter i_V^0, from 10^5 to 10^{10} A/m^3.

The activation overpotential η_{act} depends on the potential difference $\Delta\phi$ between LSM and YSZ in the composite electrode. With the assumption that ϕ_{LSM} is a constant, η_{act} becomes a function of the YSZ potential only:

$$\eta_{act} = \Delta\phi_{eq} - \Delta\phi = (\phi_{YSZ} - \phi_{LSM})_{eq} - (\phi_{YSZ} - \phi_{LSM}) \quad (15)$$
$$= \phi_{YSZ,\,eq} - \phi_{YSZ}$$

Note that the equilibrium potential $\phi_{YSZ,eq}$ depends on local chemical activities according to the Nernst equation:

$$\Delta\phi_{YSZ,\,eq} = -\frac{G}{4F} - \frac{RT}{4F} \ln\left(\frac{a(O_{2,\,gas})}{a^2(O^{2-})} \right)$$

(16)

where $a(\dots)$ stands for the activity of the species specified in brackets. We considered $a(O^{2-})$ as a constant and evaluated $a(O_{2,\,gas})$ as the ratio p_{O_2}/p_0 where p_0 is a reference pressure. By using Eq. 16 to calculate $\Delta\phi_{YSZ,\,eq}$, the concentration polarization is implicitly introduced into the model.

2.5 Simulation domain and boundary conditions

We solved the equations presented above in different 2D domains, using the commercial software COMSOL®. Imposing periodic boundary conditions on the left/right edges, domains represent repeating units. Boundary conditions are given in Table 1.

The aim of our simulations was to compare the current density from reference simulation, the flat electrode-electrolyte contact (Fig. 1, right), with the ones from structured contact simulations (Fig. 2, left).

Table 1 Boundary conditions referring to Fig. 1. ϕ_0 is total overpotential and was fixed at 0.6 V in the simulations

Variable	1	2	3	4
ϕ_{YSZ}	ϕ_0	0	Periodic	
p_{O2}	–	0.21	Periodic	
p_{N2}	–	0.79	Periodic	

Referring to Fig. 1 boundary conditions are listed in Table 1 below.

The values of parameters used in the simulations are listed in Table 2, while a summary of the constitutive equations of the model is given in Table 3.

3 Results and discussion

Two sets of stationary simulations at fixed total overpotential have been performed. In the first we fixed the geometry and varied the effectiveness factor q and the kinetic parameter i_V^0. In the second we fixed q and varied the geometry and i_V^0.

3.1 Effect of the kinetic parameter

The effect of the kinetic parameter is readily explained looking at Fig. 2 showing volumetric current density distributions. We remark that the reaction rate differs from the current density by a constant factor ($r_V = i_V/2$ F).

In the left picture, corresponding to a simulation with i_V^0 10^5 A/m^3, the reaction is spread all over the available volume. Electrochemical reaction kinetic is the limiting factor, so we will refer to similar situations as "kinetic regimes". This configuration clearly represents a non-optimized cathode, since a thicker one will show better performances, having a larger volume available for reaction.

In the right picture, corresponding to a simulation with i_V^0 10^8 A/m^3, we notice that the reaction is limited within a narrow region, close to the electrolyte. We will refer to it as the "active region", the upper part of the electrode not hosting any reaction. Increasing further the kinetic parameter will make the active zone narrower. Current density profiles at different i_V^0 and fixed overpotential can be interpreted introducing a distance a, measured from the electrode-electrolyte interface, at which the current is "almost zero" (let's call λ the ratio $i_{max}/i(a)$). This definition is clearly arbitrary, since it depends on what we consider as "almost zero", or, which is the same, from which value we approximate λ as zero. As a rule of thumb we can consider λ as zero when it reaches the value 10^{-4}. In the following we will refer to the arbitrarily determined distance a as the "active range". Simulation results of Fig. 2 show that for low i_V^0 (left) the active range a is bigger than the electrode thickness δ_{ele}, while for higher values of i_V^0 (right) a is smaller than δ_{ele}. When i_V^0 approaches infinity, a tends to zero and the active zone is ideally reduced to the surface of contact between the electrode and the electrolyte. In this case the activation overpotential will be negligible with respect to the ohmic potential drop in the electrolyte. If also the concentration overpotential is small, we'll refer to those situations as "ohmic regimes". We remark that the analysis
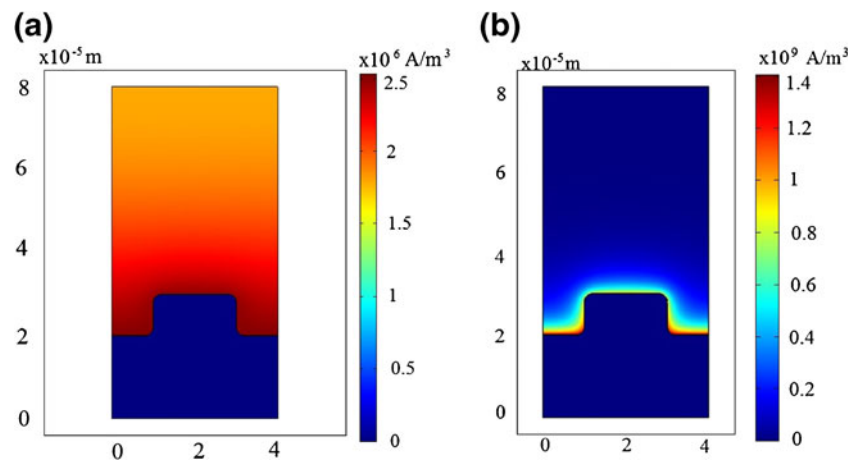
made here on the active range is valid only when all con-
ditions and parameters (total overpotential, conductivities,
gas transport parameters, etc.) are kept fixed.

3.2 Variation of effectiveness factor

We decided to explore in our simulations a whole range of
conditions, focusing in particular on material properties. In
this first set of simulations the effect of the effectiveness
factor and of the kinetic parameter has been studied. To this
aim, the geometry was fixed choosing the following

parameters: $d=10$ μm and $h=40$ μm. In the simulations i_V^0
changed on a logarithmic scale in the range 10^6–$10^{10} A/m^3$
and q between 2 and 20. The interval chosen for i_V^0 is
representative of a variety of intermediate situations be-
tween the activation and the ohmic regimes. The values
chosen for q start from 2, an optimistic improbable case,
and reach 20, value found in [15] for a volume fraction of
0.5 and a porosity of 35 %. Probably, an optimized material
will show a q close to 10.

Some results are presented in Fig. 3, where the percent-
age of current variation with respect to the reference (flat

Table 2 Model parameters		Value	Units	Reference
Constants				
	F, Faraday's constant	96485.3	C mol^{-1}	
	R, gas constant	8.314472	JK^{-1}mol^{-1}	
	α_M, symmetry factor	0.5		
Operating conditions				
	Temperature, T	1073	K	
	Outside pressure, P_{out}	1	atm	
	Outside oxygen partial pressure, P_O	0.21	atm	
Cell design parameters				
	Thickness of electrode, δ_{ele}	50	μm	
	Thickness of electrolyte, δ_{ely}	20	μm	
	Stem base	20	μm	
Material properties				
	Resistivity YSZ, ρ_{YSZ}	1.19	Ω m	[7]
	Porosity, ε	0.5	–	[1]
	Tortuosity, τ	4	–	[1]
	Mean pore radius, d_p	10^{-6}	m	
Gas phase properties				
	Oxygen viscosity, μ_O	3.2572 10^{-5}	Kg m^{-1}s^{-1}	[14]
	Nitrogen viscosity, μ_N	3.8034 10^{-5}	Kg m^{-1}s^{-1}	[14]
	Special *Fuller et al.* diffusion volume, V_N	18.5		[14]
	Special *Fuller et al.* diffusion volume, V_O	16.3		[14]

**Table 3** Summary of model equations

Pysicochemical process	Equation
Oxygen reduction kinetics	$i_V = i_V^0 \left[\exp\left(\alpha_M \frac{F}{RT} \eta_{act} \right) - \exp\left(-(1 - \alpha_M) \frac{F}{RT} \eta_{act} \right) \right]$
	$i_V^0 = i^0 \ell_{TPB}$
	$\eta_{act} = \phi_{YSZ,\,eq} - \phi_{YSZ}$
	$\Delta\phi_{YSZ,\,eq} = -\frac{\Delta G}{4F} - \frac{RT}{4F} \ln\left(\frac{a(O_{2,\,gas})}{a^2(O^{2-})} \right)$
Porous electrode gas transport	
Oxygen	$\frac{i_V}{2F} = \nabla \cdot \left(F_{o-o}^{-1} \nabla c_o + F_{o-n}^{-1} \nabla c_n \right)$
Nitrogen	$\nabla \cdot \left(F_{n-n}^{-1} \nabla c_n + F_{n-o}^{-1} \nabla c_o \right) = 0$
Potential distribution	$\frac{\sigma_{YSZ}}{q} \nabla \cdot \nabla\phi_{YSZ} = 2i_V$

contact) case $(100*(i - i_{ref})/i_{ref})$ is plotted as a function of q. Each curve corresponds to a different i_V^0. When $i_V^0 = 10^6$ A/m^3, the performance of the structured contact is worse than the flat one, except when $q>18$. Again here the cathode thickness is not optimized, because a bigger volume (*i.e.* removing the stem) would produce a higher current. The best performances for this geometry are obtained for an i_V^0 in the range 10^7–$10^8 A/m^3$. When it reaches $10^9 A/m^3$, the current is only slightly higher than the reference case and for $10^{10} A/m^3$ it falls below it. This trend is clearly due to the transition to ohmic regimes: in the structured contact design, the electrolyte has a mean thickness higher than in the reference case, so that, when electrolyte loss becomes dominant, the structured contacts show worse performances due to

the increased ohmic drop. Results of the simulation performed with an i_V^0 of $10^{10} A/m^3$ give hints for the interpretation of the phenomena. For such a high value of i_V^0, the reaction takes place in a very narrow region close to the interface. Since the increase of contact surface produced by the stems is giving worst performance, we conclude that the improvement in current density observed in our simulations is not simply due to an increase in the surface of contact between the electrode and the electrolyte.

Resuming, in activation and ohmic regimes the geometry tested is not satisfying, while, for intermediate situations, the performance increase can reach notable values, up to 45 %. Looking at current profiles, the explanation of this fact can be given in terms of the

Fig. 3 Comparison of flat and structured contacts, changing q (x-axis) and i_0^V (different curves). The relative variation of total current drawn $100*(i - i_{ref})/i_{ref}$ is plotted on the y-axis
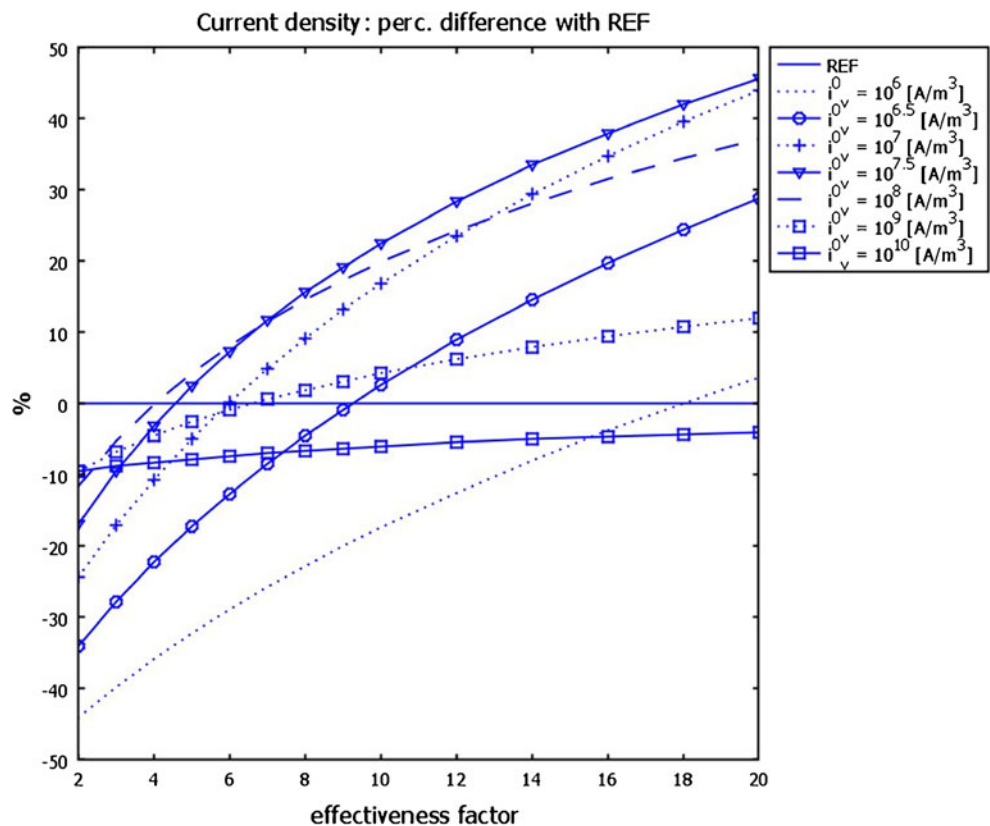
active range introduced before. In fact, the stem size $(10 \times 40 \ \mu m)$ is comparable with the active range when i_V^0 is in the interval $10^7 - 10^8 \, A/m^3$, in which the best performance amelioration is found. In other words, when the stem size is of the same order as the active range, the structured contact enhances the performance. On the contrary, a flat contact surface is preferable with respect to a structured one when the active range and the stem size are not in the same order of magnitude.

The geometry chosen – stems are tall and closely packed – does not fit for very low values of q (2–4), in the whole range of i_V^0.

3.3 Variation of geometry

The second set of simulations performed was aimed to study the effect of different contact geometries, fixing q to its

maximum value of 20 and varying i_0^V. To achieve this, we decided to vary independently the two parameters h and d that characterize the roughness, representing respectively the height of a stem and half distance between two adjacent stems, as shown in Fig. 1. The range of variation chosen was 10–40 μm for both h and d and $10^5 - 10^8 \, A/m^3$ for i_V^0.

Some results are presented in Fig. 4, where the percentage of current variation with respect to the reference case ($100*(i - i_{ref})/i_{ref}$) is plotted as a function of h. Each curve corresponds to a different value of d, as specified in the legends. In Fig. 4 A the results for $i_V^0 = 10^5 A/m^3$ are shown, close to the kinetic regime. Again we notice that performances are always worse than in the reference case, and that configurations with taller (higher h) or more compact (lower d) stems show lower current densities. This confirms the interpretation given before, i.e. the active volume is the limiting factor and is reduced by the presence of stems.
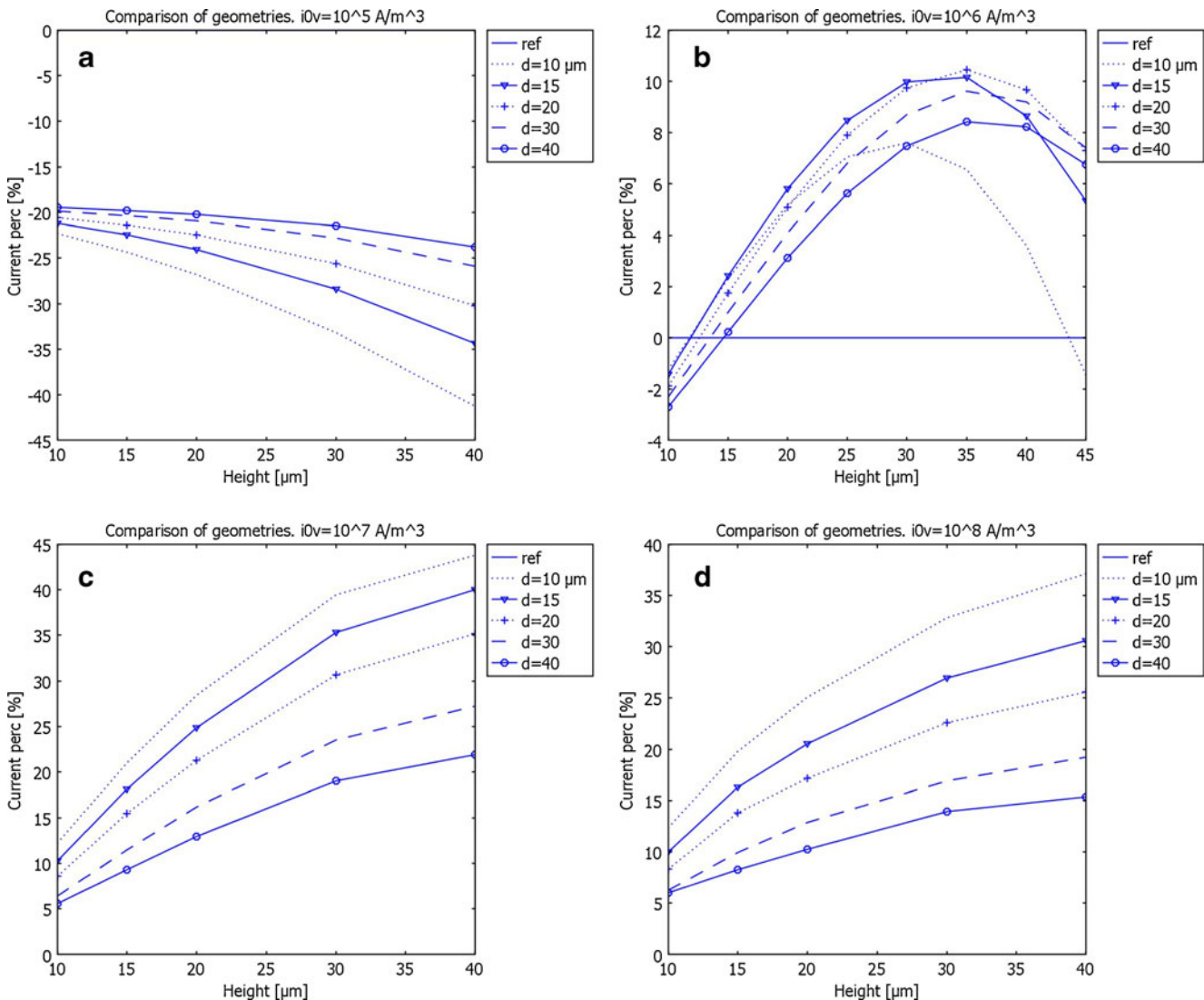
Fig. 4 Comparison between flat and structured configurations, changing h (x-axis) and d (different curves). The relative variation of total current drawn $100*(i - i_{ref})/i_{ref}$ is plotted on the y-axis. Each frame shows results at fixed i_0^V

Figure ([4b](#)) shows results for $i_V^0 = 10^6 \mathrm{A}/\mathrm{m}^3$, where the existence of an optimal choice of the geometrical parameters d and h is clearly visible. This is certainly due to a balancing between contrasting factors, *i.e.* the positive effect of the enhanced ion conduction and the negative one of the active volume reduction. A more detailed set of simulations would catch the true maximum in the range d=15–20 μm and h=30–40 μm.

Figure ([4c](#)) and ([d](#)) show results for $i_V^0 = 10^7$ and $10^8 \mathrm{A}/\mathrm{m}^3$, respectively. In both cases the best performances were obtained for high stems (h=40 μm), close to each other (d= 10 μm), for the range of geometries explored. The next step here would be to study the optimization of the size of the stem in this range of i_0^V, exploring values outside of the studied range for d and h.

4 Conclusions

The comparison between the reference flat electrolyte-electrode contact and the rough, structured one, by means of steady state finite elements simulations, showed that the latter can be advantageous in. The reason why the presence of the stem, in "intermediate" conditions when there are neither ohmic nor kinetic limitations, can increase the performance of the assembly is the fact that the stem acts as a highway for ions, being a dense conductor extending into the porous electrode. Its effect is to reduce the ohmic loss due to ionic transport in the electrode. This interpretation explains also why the stems are useful when their size is comparable with the active range (see sec. 3.1 above). We already discussed the case of kinetic regimes, where performances are lowered by the active volume reduction caused by the stems, and the case of ohmic regimes, where the stems simply increase the mean electrolyte thickness. In intermediate situations instead, losses due to ionic transport in the electrode are comparable with activation and other ohmic losses. Their reduction due the patterned contact significantly reflects into a performance increase.

A topic which will undergo future research efforts is the shape of stems. Intuition suggests that triangular sections should work better than the rectangular ones studied here, since current density gets higher closer to the electrolyte. Moreover, the possibility of pyramidal stems, even more promising, should be tested in 3D simulations.

List of symbols

a	Activity	
B	Permeability	m^{-2}
c_i	Volume concentration of species i	mol m^3
c_T	Total volume concentration in gas phase	mol m^3
E_{cell}	Cell voltage	V
D_i^K	Knudsen diffusion coefficient for species i	m^2 s^{-1}
D_{ij}^m	Binary diffusion coefficient for species i and j	m^2 s^{-1}
d	Distance between stems	m
d_p	Particle diameter	m
F	Faraday constant	C mol^1
G	Gibbs enthalpy	Jmol^{-1}
i	Macroscopic current density	A m^2
i_V	Microscopic current density	A m^3
i_V^0	Exchange current density	A m^3
ℓ_{aTPB}	Active TPB length density	m^{-2}
M_i	Molar mass of species i	Kg mol^{-1}
$\overrightarrow{N}_i$	Molar flux of species i	mol m^2 s^1
p_i	Partial pressure of species i	Pa
q	Effectiveness factor	
$<r>$	Mean pore radius	m
R	Gas constant	Jmol^{1}K^1
T	Temperature	K
S_i	Source term for species i	mol m^{-3} s^{-1}
y_i	Molar fraction of species i	
Greek letters		
α	Transfer coefficient	
δ	Thickness	m
ε	Porosity	
	Electric potential	V
η	Overpotential	V
μ	Viscosity	Pa s
ρ	Resistivity	Ω m
σ	Conductivity	Sm^1
τ	Tortuosity	
Subscripts		
eq	Equilibrium	
eff	Effective	
i	Chemical species i	
ref	Reference simulation	

References

1. S. Tao, J.T.S. Irvine, J.A. Kilner, Adv. Mater. **17**, 1734–1737 (2005)
2. J. Peña-Martinez, D. Marrero-Lòpez, D. Pèrez-Coll, J.C. Ruiz-Morales, P. Nuñez, Electrochim. Acta **52**, 2950–2958 (2007)
3. Z. Shao, S.M. Haile, Nature **431**, 170–173 (2004)
4. H. Lv, H.-y. Tu, B.-y. Zhao, Y.-j. Wu, K.-a. Hu, Solid State Ion. **177**, 3467–3472 (2007)
5. S. Tao, J.T.S. Irvine, Nat. Mater. **2**, 320–323 (2003)
6. J.B. Goodenough, Y.-H. Huang, J. Power Sourc. **173**, 1–10 (2007)

7. H. Zhu, R.J. Kee, V.M. Janardhanan, O. Deutschmann, D.G. Goodwin, J. Electrochem. Soc. **152**, A2427 (2005)

8. A. Hammouche, E.J.L. Schouler, M. Henault, Solid State Ion. **28–30**, 1205–1207 (1988)

9. J. Mizusaki, H. Tagawa, K. Naraya, T. Sasamoto, Solid State Ion. **49**, 111–118 (1991)

10. Y. Takeda, Y. Sakaki, T. Ichikawa, N. Imanishi, O. Yamamoto, M. Mari, N. Mori, T. Abe, Solid State Ion. **72**, 257–264 (1994)

11. A. Bertei, C. Nicolella, F. Delloro, W.G. Bessler, N. Bundschuh, A. Thorel, ECS Trans. **35**(1), 883 (2011)

12. Y. Ji, J.A. Kilner, M.F. Carolan, Solid State Ion. **176**, 937–943 (2005)

13. D. Arnost, P. Schneider, Chem. Eng. J. **57**, 91–99 (1995)

14. B. Todd, J.B. Young, J. Power Sourc. **110**, 186–200 (2002)

15. B. Choi, P. Kenney et al., SOFC XI ECS Trans. **25**, 1341 (2009)